Lawrence Berkeley National Laboratory
Recent Work

Title
Crystallization Behavior of a Glass in the Y{sub 2}O{sub 3}-SiO{sub 2}-AlN System

Permalink
https://escholarship.org/uc/item/16t839t1

Authors
Dinger, T.R.
Rai, R.S.
Thomas, G.

Publication Date
1987-03-01

eScholarship.org Powered by the California Digital Library
University of California

LBL-23251
Preprint

Lawrence Berkeley Laboratory
UNIVERSITY OF CALIFORNIA

Materials & Chemical Sciences Division

JUN 2 6 1987

National Center for Electron Microscopy

Submitted to Journal of the American Ceramic Society

CRYSTALLIZATION BEHAVIOR OF A GLASS IN THE Y_2O_3–SiO_2–AlN SYSTEM

T.R. Dinger, R.S. Rai, and G. Thomas

March 1987

TWO-WEEK LOAN COPY

This is a Library Circulating Copy which may be borrowed for two weeks.

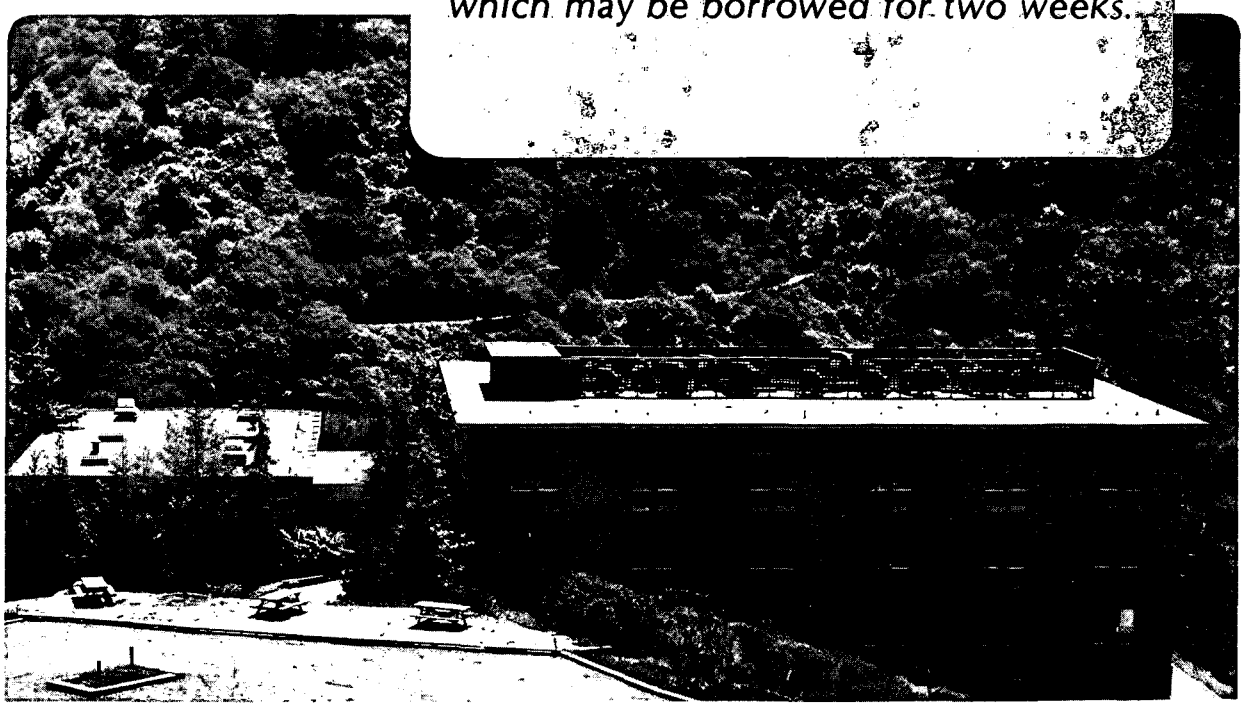

Prepared for the U.S. Department of Energy under Contract DE-AC03-76SF00098

LBL-23251

DISCLAIMER

This document was prepared as an account of work sponsored by the United States Government. While this document is believed to contain correct information, neither the United States Government nor any agency thereof, nor the Regents of the University of California, nor any of their employees, makes any warranty, express or implied, or assumes any legal responsibility for the accuracy, completeness, or usefulness of any information, apparatus, product, or process disclosed, or represents that its use would not infringe privately owned rights. Reference herein to any specific commercial product, process, or service by its trade name, trademark, manufacturer, or otherwise, does not necessarily constitute or imply its endorsement, recommendation, or favoring by the United States Government or any agency thereof, or the Regents of the University of California. The views and opinions of authors expressed herein do not necessarily state or reflect those of the United States Government or any agency thereof or the Regents of the University of California.

Crystallization Behavior of a Glass in the Y_2O_3-SiO_2-AlN System

T.R. Dinger[×]

R.S. Rai[#]

G. Thomas

Department of Materials Science and Mineral Engineering and the

National Center for Electron Microscopy,

Materials and Chemical Sciences Division,

Lawrence Berkeley Laboratory,

University of California,

Berkeley, CA 94720

[×]Now with IBM T.J. Watson Research Center, Yorktown Heights, NY 10598
[#]Now with Ohio State University, Columbus, OH 43210

Presented at the 87th Annual Meeting and Exposition of the American Ceramic Society, Cincinnati, OH, May 1985 (Basic Science Division, Paper No. 150-B-85).

Supported by the Atlantic Richfield Foundation and the National Science Foundation under Grant No. DMR 83-1317239; technical staff and support facilities were provided by the Director, Office of Energy Research, Office of Basic Energy Sciences, Materials Science Division of the U.S. Department of Energy, under Contract No. DE-AC03-76SF00098 with the University of California, Lawrence Berkeley Laboratory.

Abstract

Glass formation for a series of 10 glasses on or near the $AlN - Y_2O_3 - SiO_2$ plane of the Y-Si-Al-O-N system was found to be strongly dependent on composition with the best glass-forming characteristics occurring in a glass having a normalized composition of $Y_{0.26}Si_{0.30}Al_{0.11}ON_{0.11}$. Crystallization of this glass was found to proceed by a heterogeneous nucleation mechanism, with intermetallic iron silicides acting as nuclei for the columnar dendritic $y - Y_2Si_2O_7$ species. Secondary crystallization of a species having a nominal composition of $YSi_2AlO_4N_2$ occured in interdendritic regions when crystallization temperatures approached 1200°C. A third stage of crystallization involved the formation of the high temperature polymorph of $Y_2Si_2O_7$ ($\delta_2 - Y_2Si_2O_7$) through transformation of the $y - Y_2Si_2O_7$ dendrites to an intermediate product ($\delta_1 - Y_2Si_2O_7$) followed by recrystallization to the $\delta_2 - Y_2Si_2O_7$ polymorph. CBED results for the crystal structure determination of $y - Y_2Si_2O_7$ showed it to be based on an end-centered orthorhombic Bravais lattice having unit cell dimensions of a=8.06 Å, b=9.34 Å, and c=6.92 Å with a space group of Aba2. A similar determination for $\delta_2 - Y_2Si_2O_7$ showed it to be based on a primitive orthorhombic Bravais lattice having unit cell dimensions of a=13.6 Å, b=5.01 Å, and c=8.15 Å with a space group of $Pna2_1$.

Introduction

The recent interest in Si_3N_4-based ceramics for use in high temperature structural applications has prompted closer investigation of the glassy intergranular phases which normally exist in these materials [1]. These intergranular phases result from sintering additives or impurities contained in the raw material powders and are the cause of the invariable loss of high temperature strength [2]. Y_2O_3/Al_2O_3-fluxed Si_3N_4 is a technologically important ceramic which falls into this class of materials. The major point of interest in this system is that the intergranular glass is highly refractory and resists softening such that the useful range of the material is expanded. By formulating compositions correctly within certain compatibility triangles, it is also possible to preserve the integrity of materials in this system under high temperature oxidizing conditions [3]. Partial crystallization of the intergranular glass in Y_2O_3/Al_2O_3 -fluxed Si_3N_4 [4] by heat treatment after hot pressing has been observed with the resulting ceramic having increased creep resistance. Collectively, these points outline the advantages of Y_2O_3/Al_2O_3-fluxed Si_3N_4 for high temperature structural applications.

Oxynitride glasses have been formulated in the Y-Si-Al-O-N system by various investigators [5–10]. Heat treatment of these glasses has shown the crystallization behavior to be, in general, quite complex. Leng-Ward and Lewis [10] have discussed in detail the crystallization behavior of glasses having compositions with constant *Y:Si:Al* ratio of 1.04 : 1.27 : 1.27 and with nitrogen contents ranging from 0 to 30 eq.%. They were successful in crystallizing Si-substituted YAG (yttrium alu-

minum garnet, $Y_3Al_5O_{12}$), yttrium disilicate ($Y_2Si_2O_7$), alumina (Al_2O_3), mullite ($Al_6Si_2O_{13}$), silicon oxynitride (Si_2N_2O), and N-wollastonite ($Y_2Si_2O_4N_2$). This work is the most detailed study to date of glass crystallization in the Y-Si-Al-O-N system. Of interest in the present study was the crystallization behavior and phase analyses of glasses lying on the Y_2O_3-SiO_2-AlN plane of the Y-Si-Al-O-N system. Similar glasses had previously been fabricated by Jack [5], Loehman [6] and Thomas, Ahn and Weiss [9] who examined properties and gross crystallization phenomena. However, the crystallization behaviors of these glasses as classical glass-ceramics remained relatively unknown.

Glasses in this system have practical application as joining materials for Y_2O_3/Al_2O_3 -fluxed Si_3N_4 parts and have potential application as glass-ceramic precursors in their own right. With these applications in mind, the present work characterizes both crystallographically and morphologically some of the crystalline phases which may occur during the devitrification of glasses in the Y-Si-Al-O-N system and compares new results with those of previous investigators.

Experimental Procedures

Glass Melting

Compositions near the limits of the known glass-forming region [6] in the Y_2O_3-SiO_2-AlN system were prepared by melting mixtures of Al_2O_3, SiO_2, Y_2O_3

and Si_3N_4 powders in molybdenum crucibles in a graphite-element high temperature furnace × modified to allow pressurization to 2 MPa. This permitted a nitrogen partial pressure of approximately 2 MPa to be maintained over the melt in order to prevent decomposition of the silicon nitride during melting [11]. After holding at the melting temperature the glasses were furnace quenched by turning off the furnace. This cooling rate is approximately 60°C/minute but is strongly time dependent.

The powders were mixed using a ball mill and polyethelene containers without the addition of milling media or liquids to avoid contamination and the necessity of drying the powders after mixing. All batches were formulated as 50 g charges and were mixed for two hours .

The compositions which were prepared are shown as the lettered symbols in Figure 1. Compositions which had been prepared prior to this study are shown as numbered symbols (Loehman [6]) or are otherwise indicated (Jack [5], and Thomas, Ahn and Weiss [9]). The compositions were chosen in order to define the boundaries of the known glass-forming region in this system more precisely than those determined in earlier studies. Table I lists the compositions of the glasses formed along with the conditions used for melting and the resulting phase constitution as determined by X-ray diffraction and transmission electron microscopy. Based on these results, subsequent crystallization was limited to composition A which was

---

× Centorr Associates, Inc., Suncook, NH.

Table I

Y-Si-Al-O-N Glass Melting Results

Sample	Melting Temp. (°C)	Melting Time (hrs.)	Phase Content
A	1650	1	Amorphous*
B_1	1650	1	Amorphous#, δ-$Y_2Si_2O_7$*
B_2	1725	1	Amorphous#, δ-$Y_2Si_2O_7$*
C	1725	1	Amorphous#, β-$Y_2Si_2O_7$*
D	1725	1	Amorphous*, O'-sialon#
E_1	1725	1	Amorphous*, β'-sialon#, O'-sialon#
E_2	1725	1	Amorphous*, β'-sialon#, O'-sialon#, β-$Y_2Si_2O_7$
F	1725	1	Amorphous*, Y_2SiAlO_5N*
G	1725	1	Amorphous#, $Al_2Y_4O_9$ - J Phase (ss)*
I	1725	1	Amorphous*

*XRD Result, #TEM Result

found to be totally amorphous. Composition I, which lies near the SiO_2-rich corner of the Y_2O_3-SiO_2-AlN plane but which has an Al_2O_3 content such that its composition does not lie on this plane , resulted in a phase-separated glass similar to that reported by Leng-Ward and Lewis [10]. This phase separation is believed to be an extension of the miscibility gap which exists in the Y_2O_3- SiO_2 binary system into the AlN-SiO_2-Y_2O_3 system.

Heat Treatment

Heat treatments to effect crystallization of Y-Si-Al-O-N glass composition A were performed in a tungsten-mesh element + high temperature furnace equipped with a microprocessor-based controller # . Purified argon or nitrogen was used as the furnace atmosphere. Small pieces (< 1 g) of the bulk glass were heated in a platinum dish at a rate of 20°C/minute until a plateau temperature was reached. A cooling rate of 10°C/minute was used from the plateau temperature to room temperature.

After the establishment of the time-temperature regime in which noticeable crystallization could be achieved in reasonable times, a matrix of heat treatments was performed in order to produce a time-temperature- transformation diagram.

+ Centorr Associates Inc., Suncook, NH.
# Honeywell, Inc., Westfield, NJ.

Microstructural Characterization

Each of the crystallized glass-ceramics was characterized using the techniques of X-ray powder diffraction, scanning electron microscopy (SEM), and transmission electron microscopy (TEM). Studies performed on the transmission electron microscope included energy dispersive X-ray spectroscopy (EDXS), convergent beam electron diffraction (CBED), and high resolution electron microscopy.

X-ray powder diffraction patterns were generated on a Siemens Kristalloflex diffractometer using a 0.1 degree step size over a 2θ range of 6° to 70°. Cu Kα X-rays were used in the analyses. Powders for analyses were made by grinding the bulk glass using an agate mortar and pestle followed by sieving to 200 mesh.

SEM samples were prepared by diamond polishing bulk samples of the crystallized glass-ceramics down to 0.25 μm. These were then etched for 10 minutes using 2.0% HF acid to reveal the microstructure and coated with 5 nm of gold to prevent charging of the specimen under the influence of the electron beam. SEM was performed on a microscope operated at a 25 kV accelerating potential.

Samples for TEM were prepared by the standard techniques of thin sectioning to approximately 0.3-0.4 mm thickness using a diamond sectioning saw, grinding to approximately 50 μm using 600 grit SiC paper, and ion beam thinning using 6 keV Ar ions directed at an incidence angle of 20-25°. A thin layer of carbon (10-30 Å) was then evaporated onto one side of the specimen to reduce the effects of specimen charging. TEM observations were made in a 100 kV instrument ++

equipped with a standard energy dispersive X-ray spectrometer [***], in a 200 kV instrument [+++] equipped with an ultra-thin window energy dispersive X-ray spectrometer [****], and in the Berkeley Atomic Resolution Microscope operated at 1.0 MV.

[++] Model 400T, Philips Electronic Instruments, Mahwah, NJ.
[***] Model μ-7000, Kevex Corp., Foster City, CA.
[+++] Model JEM 200CX, JEOL Corp., Peabody, MA.
[****] Model Microanalyst-8000, Kevex Corp., Foster City, CA.

Results and Discussion

Crystallization Sequence

1000°C

Heat treatment of glass composition A at low temperatures (1000°C) resulted in very sluggish devitrification to form $y - Y_2Si_2O_7$. This identification is confirmed by X-ray diffraction results (Appendix I), which partially match the pattern generated by Ito and Johnson [12], and EDXS results which show a limited degree of solid solubility of Al (Figure 2).. To date, such solid solubility has only been documented for the case of $y - Y_2Si_2O_7$ which has a nominal composition of $R(Y,RE)_5Si_6O_{21}$ where R includes H^+, Na^+, Mg^{+2}, Mn^{+2}, Fe^{+2}, Al^{+3}, Th^{+4} *and* Zr^{+4} [12]. The partial match of X-ray diffraction patterns from this study with those of Ito and Johnson is thought to result from the occurrence of multiple crystalline species with similar structures and compositions in their study. This topic will be discussed in more detail later in this paper.

Crystallization of the $y - Y_2Si_2O_7$ phase appears to be heterogeneously nucleated as shown by the TEM micrograph of Figure 2. Such nuclei were not detected in the parent glass and probably arise due to Fe-induced reduction of Si_3N_4 during the crystallization heat treatment [13]. The source of this Fe is thought to be impurities in the raw material powders. The relatively infrequent occur-

rence of such crystallization centers tends to support the contention of a heterogeneous nucleation mechanism.

1100°C

A crystallization temperature of 1100°C or greater resulted in a dramatic increase in the crystallization rate. The secondary electron image of Figure 3(A) shows a large-scale crystallization of the $y - Y_2Si_2O_7$ phase as dendrites of approximately 20-25 μm diameter. Residual glass appears as the darker contrast phase. Small amounts of the high temperature form of $Y_2Si_2O_7$ appear in the micrograph as crystallites with the sharply angular morphology labeled δ.

The dendritic crystallization of $Y_2Si_2O_7$ has been previously observed in the surface oxide layer of hot-pressed Si_3N_4-Y_2O_3-SiO_2 materials by Babini, et al. [14], who attributed the dendrite formation to constitutional supercooling caused by a larger concentration of Y in the glass compared to stoichiometric $Y_2Si_2O_7$. In the present case the crystallization of $y - Y_2Si_2O_7$ requires the exclusion of Al, Si, O, and N to the liquid phase ahead of the glass/crystal interface, and it is this effect which causes columnar dendrite formation due to constitutional supercooling. The amount of Al which remained in solid solution in the $y - Y_2Si_2O_7$ phase was observed to decrease as a function of increasing crystallization temperature which suggests a partition coefficient which is less than 1; the functional form of this Al solubility vs. temperature relation was not determined.

1200°C

Crystallization at temperatures above about 1200°C results in a quite different morphology than that observed at lower crystallization temperatures. This morphology is characterized by the formation of a second crystalline species in the regions surrounding the $y - Y_2Si_2O_7$ dendrite nuclei. This morphology is apparent in the secondary electron image of Figure 3(B) where the interdendritic phase is shown labeled with an H. EDXS analysis of this devitrification product shows it to contain all five of the elemental constituents of the system. Using $Y_2Si_2O_7$ and Y_2SiAlO_5N [15] as standards for determining Cliff-Lorimer coefficients, a nominal composition of $YSi_2AlO_4N_2$ was calculated for the interdendritic phase. A quinary composition such as this might be expected since Al, Si, O, and N are segregated to the regions between the dendrites. Observations of the $YSi_2AlO_4N_2$ phase in the transmission electron microscope confirm its existence in the regions surrounding the dendrite nucleus and radiating dendrite arms. In fact, Figure 4 suggests that the growth of $YSi_2AlO_4N_2$ proceeds in a single crystal fashion until envelopment of the dendrite has occurred. The (001) lattice fringes of the $YSi_2AlO_4N_2$ phase completely surround the twin-faulted dendrite arm seen here in a cross-sectional orientation.

The stoichiometric compound Y_2SiAlO_5N and the series of solid solutions which form between the compositions $Y_4Si_2O_7N_2$ and $Y_4Al_2O_9$ are the only reported quinary compounds in the Y-Si-Al-O-N system [15] These compounds are both Y-rich compared to the interdendritic phase of this study which suggests that we

have identified a previously uncataloged crystalline species. Diffraction results to follow also suggest this.

>1200°C

Heat treatment at crystallization temperatures in excess of 1200°C gave rise to a monotropic transformation microstructure which results from the formation of the stable high temperature polymorphs of $Y_2Si_2O_7$ or the δ forms. This morphology is easily observed in the transmission electron micrograph of Figure 5 in which the δ_2 polymorph exhibits a blocky morphology containing many faults and can be seen growing from what were originally $y - Y_2Si_2O_7$ dendrite branches. The assignment of $\delta_2 - Y_2Si_2O_7$ as the description of the polymorph formed in this transformation is based on the description of the δ polymorph by Ito and Johnson [12] and the similarity of X-ray and electron diffraction patterns from the δ_1 and δ_2 polymorphs (Appendix II) to a pattern produced by Ito and Johnson [16]. The complexity of this $y \rightarrow \delta$ transformation will be discussed further in the following section.

Heat treatment of glass composition A at high temperatures for long periods of time resulted in the microstructure observed in the secondary electron micrograph of Figure 3(B). This microstructure consists entirely of the $\delta_2 - Y_2Si_2O_7$ polymorph (δ_2), the $YSi_2AlO_4N_2$ phase (H), O' sialon needles (O'), and some amount of residual glassy phase which appears as the angular regions of dark contrast found between the $\delta_2 - Y_2Si_2O_7$ crystallites. Precipitation of O' sialon

needles from Y-Si-Al-O-N glasses has also been observed by Leng-Ward and Lewis [10] for heat treatments at or above 1250°C. Nucleation of this phase generally occurred after the composition of the residual glass had been enriched in nitrogen following the crystallization of $Y_3Al_5O_{12}$ (YAG). In the present cases, the precipitation of O' sialon followed the crystallization of $Y_2Si_2O_7$ which also increases the nitrogen content of the residual glass.

The crystallization behavior of the Y-Si-Al-O-N glass presented here is summarized in the qualitative time-temperature-transformation (TTT) diagram of Figure 6. No finish curve is indicated for the glassy phase since SEM analyses of HF-etched specimens showed glass to be present in some detectable amount in all instances. Those areas of the diagram which are poorly defined are indicated by dashed lines. No distinction is made on this diagram between the δ_1 and δ_2 polymorphs because morphological and structural similarity make accurate detection by SEM and X-ray diffraction difficult. A detailed description of some of the aspects of the $\delta_1 - Y_2Si_2O_7$-$\delta_2 - Y_2Si_2O_7$ crystallization will now be presented.

Intergrowth of $\delta_1 - Y_2Si_2O_7$ and $\delta_2 - Y_2Si_2O_7$

As pointed out earlier in this work, the crystallization of glass composition A occurs via a dendritic mechanism. Initially, dendrites consisting of the y polymorph of $Y_2Si_2O_7$ crystallize during the heating ramp, but heat treatment at higher temperatures results in the transformation of y-phase into two similar

structures, i.e. the δ-phases of $Y_2Si_2O_7$. Both are orthorhombic with the same unit cell parameters but different space groups, however no structural details of δ-phases are reported in the literature. The major problem is the high degree of polymorphism exhibited by $Y_2Si_2O_7$. Additional problems resulted in this study due to microtwinning in the primary and secondary dendrite arms as well as faulting in the secondary arms. Therefore, attempts to characterize the structural details of the δ-phases by X-ray diffraction have failed due to averaging effects. We describe the two transformed structures from y-phase dendrites as $\delta_1 - Y_2Si_2O_7$ and $\delta_2 - Y_2Si_2O_7$.

Figure 7 shows an example of the dendritic morphology of the δ-phases in a matrix of residual glass. The primary arm of the dendrite consists of $\delta_1 - Y_2Si_2O_7$ which is microtwinned (dark lines marked with a T in the region of the primary arm of the dendrite). The angular crystallites attached to the primary arms, i.e. secondary arms, of the dendrites consist of both δ-phases together with faulted regions due to the intergrowth, although the majority of the secondary arms consist of $\delta_2 - Y_2Si_2O_7$. It is interesting to note that the secondary arms of the dendrites maintain the orientations of the twin variants of the primary arm. The terminations of the faults (marked with an F in Figure 7) inside the primary arms indicate the nucleation of $\delta_2 - Y_2Si_2O_7$ as a result of faulting. Electron diffraction patterns (Figure 8(A)) from a region encircled in Figure 7 were complex arising from four sets of oriented crystallites. Of these four sets, two correspond to twinned $\delta_1 - Y_2Si_2O_7$ (primary arm of the dendrite) while the other two correspond to $\delta_2 - Y_2Si_2O_7$ crystallites (secondary arms of the dendrites). The electron

diffraction pattern generated is shown in Figure 8(A) and the schematic for generation of this [001] pattern is shown in Figure 8(B). Another orientation in which twinning of the primary arm of the dendrite was found is $[\bar{1}\bar{1}2]$. Twins were not found in $[0\bar{1}1]$ and $[0\bar{2}1]$ orientations. The twin plane was found to be (110). Figure 9(A) shows a high resolution electron micrograph from an interface of primary and secondary arms of the dendrite. The primary arm due to $\delta_1 - Y_2Si_2O_7$ clearly shows twin-related regions while the secondary arm is largely composed of $\delta_2 - Y_2Si_2O_7$. The difference in the atomic arrangements of the two structures is visible. An interesting example of the interface between primary and secondary arms of the dendrite is shown in the high resolution electron micrograph of Figure 9(B). Again the primary arm exhibits twin-related regions but in this case strain contrast due to dislocations (arrowed) at the interface is visible. This is an interesting example of epitaxial growth in which the flat faces, (100) $\delta_1 - Y_2Si_2O_7$ || (100) $\delta_2 - Y_2Si_2O_7$ are incoherent twin boundaries showing good registry but with a detectable strain field. Where $\delta_1 - Y_2Si_2O_7$ is twinned, the region ~ 250 Å from the $\delta_1 - Y_2Si_2O_7/\delta_2 - Y_2Si_2O_7$ interface (i.e. the secondary/primary arm interface) is distorted and faulted. This indicates that growth of $\delta_2 - Y_2Si_2O_7$ in the secondary arm from twinned $\delta_1 - Y_2Si_2O_7$ in the primary arm is controlled by a dislocation mechanism. The exact nature of the dislocation mechanism involved in the growth of $\delta_2 - Y_2Si_2O_7$ from $\delta_1 - Y_2Si_2O_7$ is not clearly understood, but it suggests that nucleation of $\delta_2 - Y_2Si_2O_7$ is difficult.

Figure 10 shows an example of the parallel intergrowth of $\delta_1 - Y_2Si_2O_7$ and $\delta_2 - Y_2Si_2O_7$ in the [001] orientation from a region within a secondary arm of the

dendrite. Some fault positions (marked with an F) are also seen in the image. These positions do not correspond to either of the δ structures and, hence, are stacking faults; the stacking fault plane was found to be (100). A periodic arrangement of dot patterns (black and white) at 1.36 nm (corresponding to the a-parameter of $\delta_2 - Y_2Si_2O_7$) is present in the $\delta_2 - Y_2Si_2O_7$ region of the image whereas in the $\delta_1 - Y_2Si_2O_7$ region periodic arrangement is at 0.68 nm (corresponding to the a/2 spacing of $\delta_1 - Y_2Si_2O_7$) while there is a b/2 shift in the two arrangements. The structural difference in the two regions of the image is clearly seen from the arrangement of the dot patterns. Figure 11(A) shows a high resolution electron micrograph in $[0\bar{1}1]$ from a region of the secondary arm of the dendrite. Again in $[0\bar{1}1]$, the two structures grow in a parallel orientation relationship. The insets in Figure 11(A) are laser optical diffractograms corresponding to the two regions. In the $\delta_2 - Y_2Si_2O_7$ region a periodicity of 1.36 nm is present whereas in $\delta_1 - Y_2Si_2O_7$ the periodicity is 0.68 nm and the shift in the arrangement of the dot patterns is 1/2 [011]. Figure 11(B) shows another example of the parallel intergrowth of the two δ structures in the $[0\bar{2}1]$ orientation from a region of the secondary arm of a dendrite. The insets in Figure 11(B) are optical diffractograms corresponding to the two δ structures. Again, the basic difference of the two structures in this orientation is clear from the arrangement of dot patterns. That is, a periodicity of 1.36 nm in the $\delta_2 - Y_2Si_2O_7$ region versus a periodicity of 0.68 nm in the $\delta_1 - Y_2Si_2O_7$ region followed by a shift of 1/2 [012].

Thus, from the X-ray diffraction and high resolution micrographs taken in the orientations shown above (showing the parallel intergrowth of the two struc-

tures), it was possible to resolve the structural differences of $\delta_1 - Y_2Si_2O_7$ and $\delta_2 - Y_2Si_2O_7$. For h00 and 0k0 reflections, systematic absences were found for h=2n+1 and k=2n+1 in both cases. In the case of $\delta_1 - Y_2Si_2O_7$ systematic absences for hk0 reflections were found for h+k=2n+1, whereas in the case of $\delta_2 - Y_2Si_2O_7$, no structural extinctions were found for hk0-type reflections. Thus the space groups of the two phases are different. In this study, $\delta_2 - Y_2Si_2O_7$ was found to be isostructural with $Gd_2Si_2O_7$ [17] with detailed structural information on $\delta_2 - Y_2Si_2O_7$ to be described below including convergent beam electron diffraction data. Further structural details of the δ-phases of $Y_2Si_2O_7$ observed using high resolution electron microscopy are extremely sensitive to experimental parameters and any useful information is obtained under only the most suitable and controlled imaging imaging conditions. Such an analysis requires the use of computer simulations such as those described by Cowley and Moodie [18]. A detailed account of the results from a simulation of the atomic imaging analysis of δ_2 is reported elsewhere [19]. However, it is important to note that the high resolution images referred to in the present paper have all been interpreted with such simulation techniques.

The parallel intergrowth of the two structures observed in the secondary arms of the dendrites suggests that this type of microstructure is characteristic of an intermediate stage of transformation between the δ_1 and δ_2 forms of $Y_2Si_2O_7$. This is consistent with the observation that glass crystallized around 1300-1400°C produced mainly the δ_2 form, which suggests that $\delta_1 - Y_2Si_2O_7$ is the low temperature polymorph whereas $\delta_2 - Y_2Si_2O_7$ is the high temperature form. Similar types

of microstructures have been reported by other workers [20–22] in high resolution electron microscopic studies of intermediate $\beta \rightarrow \alpha$ transformations in SiC.

CBED and X-ray Diffraction

The simultaneous occurrence of three quite similar crystalline species in the glass-ceramic described here has confused the interpretation of the X-ray powder diffraction patterns acquired. Convergent beam electron diffraction (CBED) using the techniques described by Buxton et al. [23], has been used to determine the crystallography of individual crystallites in the partially crystallized glass-ceramic.

Figure 12 shows the [001] zone axis pattern for $y - Y_2Si_2O_7$. Parts (B) and (C) of the figure are enlargements of the two mirror planes which cut the first order Laue zone (FOLZ) ring normal to [100] and [010], respectively. Most interesting is the "double" FOLZ ring which occurs; closer examination of Figure 12(C) shows that the FOLZ has twice the density of reciprocal lattice points as the zero order Laue zone (ZOLZ). Such a phenomenon can only occur under dynamical scattering conditions [23]. The occurrence of these doubly-diffracted discs at kinematically forbidden positions necessitates a unit cell whose dimension in the [010] direction is twice that measured. Superposition of the discs in the zero and second Laue zones requires a non-primitive unit cell, and this cell has been determined to be base-centered on the (100) plane with cell dimensions of a=8.06 Å, b=9.34 Å, and c=6.92 Å.

For a point group of mm2, the systematic absences h00: h=2n and 0kl: k=2n; l=2n narrow the space group choice to Aba2. The dark bars observed in the (100) systematic row of Figure 12(A) for reflections in which h≠2n occur due to the a-type glide plane normal to [010] [25]. For the case of an mmm point group, convention places the base-centering operation on the (110) plane. Rearranging indices and observing the systematic absences 00l: l=2n and hk0: h=2n; k=2n, the space group could be determined to be Cmca, with the dark bars in the figure arising due to the c-glide plane normal to [010]. Distinguishing between Aba2 and Cmca space groups is based on a point group determination between mm2 and mmm. Buxton et al. [23] have determined that in order to distinguish between these two point groups using CBED, dark field patterns must be analyzed. The distinguishing feature is that the internal symmetry for a special dark field reflection (i.e. one lying on a symmetry element) of point group 2mm is m, while for point group mmm the internal symmetry is 2mm. Similarly, the internal symmetry of a general dark field reflection for point group 2mm is 1 while that for point group mmm is m. Dark field images for the present case yielded m symmetry for special reflections and 1 symmetry for general reflections, confirming mm2 as the point group and determining Aba2 as the space group for $y - Y_2Si_2O_7$. These results have been confirmed by real-space analysis of atomic resolution images of the δ_2 phase. [19]

Crystallographic characterization of the high temperature polymorph of $Y_2Si_2O_7$ or $\delta_2 - Y_2Si_2O_7$ using CBED was complicated by the intergrowth of

$\delta_1 - Y_2Si_2O_7$. The [010] zone axis CBED pattern of Figure 13(A) along with the enlargements of the FOLZ ring along [001] and [100] shown in parts (B) and (C), respectively, reveal the presence of a mirror plane in (B) for [100] only. Extension of the zero order Laue zone to the first order Laue zone (FOLZ) ring shows total overlap of the discs. This observation, in conjuction with measurements of the diameter of the FOLZ ring [26], is sufficient to establish the Bravais lattice as primitive orthorhombic. Subsequently, unit cell dimensions of a=13.60 Å, b=5.01 Å, and c=8.15 Å were used to generate the X-ray powder diffraction pattern observed (Appendix II). Systematic absences for 0kl: k+l=2n+1 and h0l: h=2n+1 unambiguously result in a space group of $Pna2_1$ for $\delta_2 - Y_2Si_2O_7$ [27]. Similar results have been obtained for the high temperature forms of several other rare-earth silicates based on X-ray data [28].

Crystallographic characterization of the quinary $YSi_2AlO_4N_2$ phase has been troubled by several details. Of primary significance is the fact that the similarity of the unit cell of $YSi_2AlO_4N_2$ to the unit cells of the $Y_2Si_2O_7$ phases causes considerable overlap in the X-ray diffraction patterns. $YSi_2AlO_4N_2$ crystallizes from this glass as a consequence of the crystallization of $Y_2Si_2O_7$; hence, these two crystalline species always occur in this particular glass-ceramic composition in conjunction with one another. Limited CBED results and high resolution electron microscopy show this species to have orthorhombic symmetry with unit cell dimensions of a=23.1 Å, b=5.01 Å, and c=8.06 Å (Figure 14). Present in this pattern is 2mm symmetry which is consistent with the orthorhombic system; details within the disks are washed out due to either the overlap of the discs caused

by the large interplanar spacing in [100], large numbers of point defects in the crystal, or the thinness of the crystal. The first order Laue zone of the crystal, not shown in Figure 14, also exhibits 2mm symmetry which confirms the crystal system as orthorhombic.

Conclusions

A study of the sequences involved in the crystallization of a glass on the $Y_2O_3 - SiO_2 - AlN$ plane of the Y-Si-Al-O-N system has resulted in morphological descriptions and space group and structure determinations for the polymorphs of $Y_2Si_2O_7$ which occur during heat treatments varying in both duration and crystallization temperature. The formation of a previously undocumented quinary Y-Si-Al-O-N phase also occurred and a partial structure determination of this phase has been performed.

Glass formation for a series of 10 glasses on or near the $Y_2O_3 - SiO_2 - AlN$ plane of the Y-Si-Al-O-N system was found to be strongly dependent on composition with the best glass-forming characteristics occurring in a glass having a normalized composition of $Y_{0.26}Si_{0.30}Al_{0.11}ON_{0.11}$.

Crystallization of this glass at relatively low temperatures (1100°C) was found to proceed by a heterogeneous nucleation mechanism, with intermetallic iron silicides acting as the heterogeneous nuclei. $y - Y_2Si_2O_7$ was observed to grow in a columnar dendritic morphology from these centers, with the most rapid crystallization rates occurring in the 1100°C-1200°C temperature range. CBED and X-ray diffraction have shown this crystal to be based on an a-centered orthorhombic Bravais lattice having unit cell dimensions of a=8.06 Å, b=9.34 Å, and c=6.92 Å with a space group of Aba2.

Secondary crystallization of a species having a nominal composition of $YSi_2AlO_4N_2$ occurs in regions of the microstructure rich in Al and N for temper-

atures approaching 1200°C. This species is based on an orthorhombic unit cell having dimensions of a=23.1 Å, b=5.01 Å, and c=8.06 Å. Identification of this species was not possible based on known quinary compounds in this system. The results indicate that growth of the dendritic y-phase is accompanied by rejection of Al and N to the interdendritic glass until the composition reaches that of the yttrium-silicon-aluminum oxynitride phase whence crystallization follows.

A third regime of the crystallization sequence involves the nucleation and growth of the high temperature polymorph of $Y_2Si_2O_7$ ($\delta_2 - Y_2Si_2O_7$) through transformation of the $y - Y_2Si_2O_7$ dendrites to $\delta_1 - Y_2Si_2O_7$ followed by recrystallization to the $\delta_2 - Y_2Si_2O_7$ polymorph. CBED and X-ray diffraction results for the crystal structure determination of $\delta_2 - Y_2Si_2O_7$ confirm that the structure is based on a primitive orthorhombic Bravais lattice having unit cell dimensions of a=13.6 Å, b=5.01 Å, and c=8.15 Å with a space group of $Pna2_1$.

The primary arms of the dendrites were found to consist of microtwinned $\delta_1 - Y_2Si_2O_7$ having (110) as the twinning plane. The secondary arms of the dendrites consist of a mixture of $\delta_1 - Y_2Si_2O_7$ and $\delta_2 - Y_2Si_2O_7$ as well as numerous stacking faults. The stacking fault plane was found to be (100). The absence of twinning and only occasional faulting in $\delta_2 - Y_2Si_2O_7$ indicates that it has a more highly ordered structure than does $\delta_1 - Y_2Si_2O_7$. The existence of $\delta_2 - Y_2Si_2O_7$ as the predominant species in glass crystallized at high temperatures (1300-1400°C) suggests that this polymorph is the high temperature form.

Acknowledgements

The authors would like to thank Drs. Sylvia Johnson and David Rowcliffe of the Stanford Research Institute and Dr. M.J. O'Keefe, Dr. Brian Dalgleish, Dr. Tadeusz Bielicki, Mr. Chuck Echer and Ms. Kathy Louie of the Lawrence Berkeley Laboratory for experimental assistance and helpful discussions.

Appendices

Appendix I: X-ray Diffraction Pattern for y – $Y_2Si_2O_7$

Crystal System: Orthorhombic
Space Group: Aba2
Cell Parameters: a = 8.06 Å
b = 9.34 Å
c = 6.92 Å

d_{obs} (Å)	*Intensity*	$d_{calculated}$ (Å)	*hkl*
4.67	m	4.67	020
4.03	m	4.03	200
		4.04	120
3.46	s	3.46	002
3.05	vs	3.05	220
2.63	s	2.63	202
2.34	w	2.34	040
2.02	m	2.02	240
		2.02	400
1.86	w	1.86	420
1.74	s	1.74	004
1.59	w	1.59	204
1.37	w	1.37	044

Appendix II: X-ray Diffraction Pattern for $\delta_2 - Y_2Si_2O_7$

ASTM Powder Diffraction File Card No. 20-1460

Crystal System: Orthorhombic
Space Group: $Pna2_1$
Cell Parameters: a = 13.6 Å
b = 5.01 Å
c = 8.15 Å

d_{obs} (Å)	*Intensity*	$d_{calculated}$ (Å)	*hkl*
5.23	10	5.22	201
4.70	6	4.70	110
4.07	70	4.07	002
4.05	30	4.07	111
4.03	10	4.03	210
3.61	30	3.61	211
3.41	50	3.40	400
3.36	3	3.36	310
3.08	80	3.07	112
2.87	100	2.86	212
2.61	50	2.60	402
2.39	4	2.39	510
2.19	4	2.18	601
2.13	10	2.13	022
2.11	30	2.11	122
2.07	40	2.07	512
2.04	30	2.04	004
2.02	10	2.02	420
1.93	20	1.93	322
1.84	20	1.85	612
1.82	30	1.81	422
1.75	20	1.74	314
1.68	10	1.66	130
1.65	5	1.65	414
1.57	20	1.57	124
1.53	20	1.53	132

References

References

1. D.R. Clarke and G. Thomas, "Microstructure of Y_2O_3 Fluxed Hot-Pressed Silicon Nitride," J. Am. Cer. Soc. 61 [3-4], 114-118 (1978).

2. D.W. Richerson, "Effect of Impurities on the High Temperature Properties of Hot-Pressed Silicon Nitride," Bull. Am. Cer. Soc. 52 [7], 560-562, 569 (1973).

3. F.F. Lange, S.C. Singhal and R.C. Kuznicki, "Phase Relations and Stability Studies in the Si_3N_4-SiO_2-Y_2O_3 Pseudoternary System," J. Am. Cer. Soc. 60 [5-6], 249-252 (1977).

4. A.W.J.M Rae, D.P. Thompson, H.J. Pipkin and K.H. Jack, "Special Ceramics", Vol. 6, edited by P. Popper, British Ceramic Research Association, Stoke-on-Trent, 1975, p. 283.

5. K.H. Jack, "Sialon Glasses," in Special Ceramics, Vol. 6, edited by P. Popper, British Ceramic Research Association, Stoke-on Trent, 1975, pp. 257 -62.

6. R.E. Loehman, "Preparation and Properties of Yttrium-Silicon-Aluminum Oxynitride Glasses," J. Am. Cer. Soc. 62 [9-10], 491-494 (1979).

7. D.R. Messier, "Preparation and Crystallization of Si-Y-Al-O-N Glasses," Cer. Eng. Sci. Proc. 3 [9-10], 565-576 (1982).

8. R. Shillito, R.R. Wills and R.B. Bennett, "Silicon Metal Oxynitride Glasses," J. Am. Cer. Soc. 61 [11-12], 537 (1978).

9. G. Thomas, C. Ahn and J. Weiss, "Characterization and Crystallization of Y-Si-Al-O-N Glass," Comm. Am. Cer. Soc. 65 [11], C-185-188 (1982).

10. G. Leng-Ward and M.H. Lewis, "Crystallization in Y-Si-Al-O-N Glasses," Mat. Sci. and Eng. 71 , 101-111 (1985).

11. R.E. Loehman, "Oxynitride Glasses," J. Non-Cryst. Sol. 42 , 433-446 (1980).

12. J. Ito and H. Johnson, "Synthesis and Study of Yttrialite," Am. Mineral. 53 , 1940-1952 (1968).

13. R.E. Loehman, "Preparation and Properties of Oxynitride Glasses," J. Noncryst. Sol. 56 , 411-416 (1983).

14. G.N. Babini, A. Bellosi, and P. Vincenzini, "Factors Influencing Structural Evolution in the Oxide of Hot-Pressed Si_3N_4-Y_2O_3- SiO_2 Materials," J. Mat. Sci. 19 , 3487-3497 (1984).

15. K.H. Jack, "The Role of Additives in the Densification of Nitrogen Ceramics," Final Technical Report, April-October 1977, European Research Office, United States Army, Grant No. DAERO-76-G-067.

16. JCPDS X-ray Powder Diffraction File, Card No. 21-1460.

17. Yu I. Smolin and Yu F. Shepelev, "The Crystal Structure of Rare Earth Pyrosilicates," Acta Cryst. B26 , 484-492 (1970).

18. J.M. Cowley and A.F. Moodie, "The Scattering of Electrons by Atoms and Crystals: I, A New Theoretical Approach," Acta Cryst. 10 , 609-619 (1957).

19. R.S. Rai, M.J. O'Keefe and G. Thomas, submitted to Proceedings Symposium I, "Defect Characterization," Materials Research Society, 1986 Fall Meeting, Boston, MA, Dec. 1-6, 1986.

20. D.J. Smith, N.W. Jepps and T.F. Page, "Observation of Silicon Carbide by High Resolution Electron Microscopy," J. Microscopy, 114 , 1-18 (1978).

21. N.W. Jepps and T.F. Page, "Intermediate Transformation in Silicon Carbide," J. Microscopy, 119 , 177-188 (1980).

22. L.U. Ogubuji, T.E. Mitchell, A.H. Heuer and S. Shinozaki, "The β -α Transformation in Polycrystalline SiC: IV, A Comparison of Conventionally Sintered, Hot Pressed Reaction-Sintered and Chemically Vapor Deposited Samples," J. Am. Cer. Soc. 64 , 91-99 (1981).

23. B.F. Buxton, J.A. Eades, J.W. Steeds, and G.M. Rackham, "The Symmetry of Electron Diffraction Zone Axis Patterns," Phil. Trans. Roy. Soc. London A281 , 171-194 (1976).

24. J.W. Steeds, "Convergent Beam Electron Diffraction," Chapter 15 of Introduction to Analytical Electron Microscopy : J.J Hren, J.I. Goldstein, and D.C. Joy (eds.), Plenum Press, New York, 1979, p. 387.

25. J. Gjonnes and A.F. Moodie, "Extinction Conditions in the Dynamic Theory of Electron Diffraction," Acta Cryst. 19 , 65-67 (1965).

26. See for example. D.B. Williams, Practical Analytical Electron Microscopy in Materials Science : Philips Electronic Instruments, Inc., Mahwah, NJ, 1984, p. 121.

27. International Table for X-ray Crystallography, Volume I: Symmetry Groups: N.F.M. Henry and K. Lonsdale (eds.), The Kynoch Press, Birmingham, England, 1969, p. 119.

28. J. Felsche and W. Hirsiger, "The Polymorphs of the Rare-Earth Pyrosilicates $R.E._2Si_2O_7$, [R.E.: La, Ce, Pr, Nd, Sm]," J. Less-Common Metals 18 , 131-137 (1969).

Figure Captions

Figure 1. AlN-SiO_2-Y_2O_3 ternary system showing the compositions investigated (lettered symbols). Compositions which lie in this plane and have been investigated by other are also indicated, with glasses studied by Loehman [10] being shown as numbered symbols. Composition I is an Al_2O_3-containing glass and, therefore, does not lie on the section as shown. The position indicated is the projection of composition I onto the ternary section.

Figure 2. Bright field transmission electron micrograph of a heterogeneously-nucleated crystallite of $y - Y_2Si_2O_7$ (indicated by a "2" and showing a corresponding EDX spectrum) formed on an intermetallic Fe-silicide particle (indicated by a "1" and showing a corresponding EDX spectrum).

Figure 3. (A) Secondary electron micrograph of an HF-etched specimen of Y-Si-Al-O-N glass composition A after heat treatment at 1250°C for 10 minutes. The dendritic morphology of the $y - Y_2Si_2O_7$ (labeled y) is readily observed. Small amounts of the high temperature form of $Y_2Si_2O_7$ or $\delta_2 - Y_2Si_2O_7$ (labeled δ) are beginning to form. This phase is identifiable in the SEM micrograph by its angular morphology. (B) Secondary electron micrograph of an HF-etched specimen of Y-Si-Al-O-N glass composition A after heat treatment at 1275°C for 31.6 minutes. Growth of the $YSi_2AlO_4N_2$ (H) phase in regions surrounding dendrite nuclei is observed as is the appearance of small amounts of the $\delta_2 - Y_2Si_2O_7$ (δ) phase.

(C) Secondary electron micrograph of an HF-etched specimen of Y-Si-Al-O-N glass composition A after heat treatment at 1300°C for 1000 minutes. The dendritic $y - Y_2Si_2O_7$ phase has been completely transformed to the δ_2 phase which is stable at high temperatures. The $YSi_2AlO_4N_2$ phase remains present and O' sialon needles have begun to form.

Figure 4. High resolution electron micrograph of a twinned $\delta_1 - Y_2Si_2O_7$ dendrite arm completely enveloped by the (001) lattice fringes of the $YSi_2AlO_4N_2$ interdendritic phase.

Figure 5. Bright field transmission electron micrograph of the quenched-in monotropic transformation microstructure of glass composition A after heat treatment at 1250°C for 100 minutes. The image shows the growth of the δ_2 polymorph of $Y_2Si_2O_7$ (blocky, faulted crystallites) growing from the original dendrite branches (crystallites showing a smooth crystal/glass interface such as that extending from the bottom, right-hand corner of the micrograph).

Figure 6. Qualitative time-temperature-transformation (TTT) diagram for Y-Si-Al-O-N glass composition A indicating the starting curves for the formation of $y - Y_2Si_2O_7$, $\delta - Y_2Si_2O_7$, $YSi_2AlO_4N_2$, and O' sialon and the finishing curve for $y - Y_2Si_2O_7$. No distinction between the δ_1 and δ_2 phases is made here. Poorly defined boundaries are designated by dashed lines.

Figure 7. Transmission electron micrograph showing the dendritic morphology of $\delta_1 - Y_2Si_2O_7$ and $\delta_2 - y_2Si_2O_7$ in the matrix of residual glass. Some faults terminating in the primary arm of the dendrite are marked as F. Some twins are marked as T.

Figure 8. (A) Selected area electron diffraction pattern from a twinned area of $\delta_1 - Y_2Si_2O_7$, i.e. from a region of the primary arm in the [001] orientation with contributions from the secondary arms of the dendrite in the [001] orientation. (B) Schematic electron diffraction pattern from a region encircled in Figure 7. Four spot patterns are present of which two correspond to twinned δ_1 (marked) and two which occur due to the side arms of the dendrite which are mainly δ_2 (marked).

Figure 9. (A) High resolution electron micrograph from an interface of primary (δ_1) and secondary (δ_2) arms in the [001] orientation. The twin-related regions in δ_1 are clearly observed. (B) High resolution electron micrograph showing the interface of δ_1 and δ_2 from a region of primary and secondary arms. Strain contrast due to dislocations is arrowed at several places.

Figure 10. High resolution electron micrograph showing parallel intergrowth of δ_1 and δ_2 from a region of secondary arm of a dendrite in the [001] orientation. Some stacking fault positions are marked as F.

Figure 11. (A) High resolution electron micrograph showing parallel intergrowth of δ_1 and δ_2 in the $[0\bar{1}1]$ orientation. The insets are laser optical diffractograms. (B) High resolution electron micrograph showing parallel intergrowth of δ_1 and δ_2 in the $[0\bar{2}1]$ orientation. The δ_1 and δ_2 regions are marked. The insets are optical diffractograms.

Figure 12. (A) [001] zone axis CBED pattern for $y - Y_2Si_2O_7$ revealing Gjonnes-Moodie lines in h00: h=2n+1. (B) Enlargement of the FOLZ ring along [100] showing mirror symmetry for [010]. (C) Enlargement of the FOLZ ring along [010] showing mirror symmetry for [100].

Figure 13. (A) [010] zone axis CBED pattern for $\delta_2 - Y_2Si_2O_7$ revealing Gjonnes-Moodie lines in 00l: l=2n+1. These "dark bars" occur in kinematically forbidden reflections and indicate the presence of an 2-fold screw axis along [001]. (B) Enlargement of the FOLZ ring along [001] showing mirror symmetry for [100]. (C) Enlargement of the FOLZ ring along [100].

Figure 14. Zero-order Laue zone microdiffraction pattern taken from the [001] orientation of the $YSi_2AlO_4N_2$ interdendritic phase. Little structural information is available in the overlapping disks of the pattern, but orthorhombic 2mm symmetry is suggested by the diffuse FOLZ ring (not shown).

Figures

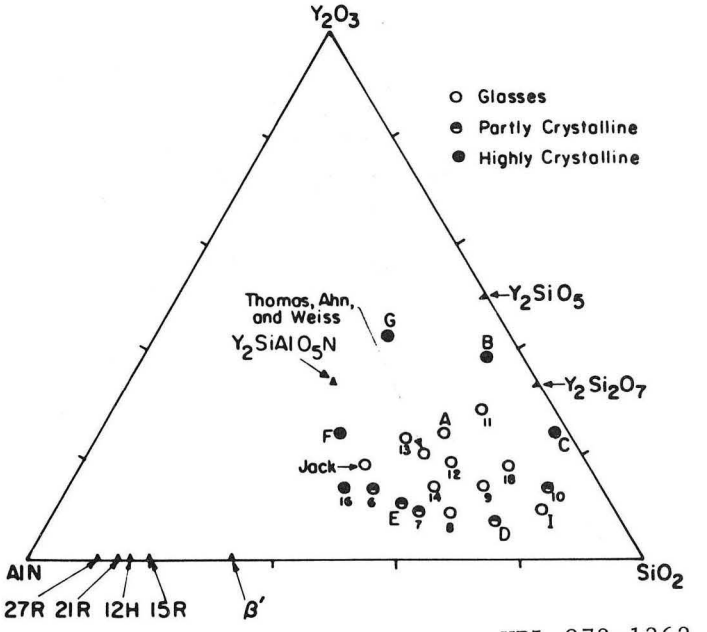
Y_2O_3
Glasses
Partly Crystalline
Highly Crystalline
Thomas, Ahn, and Weiss
Y_2SiAlO_5N
G
Y_2SiO_5
B
$Y_2Si_2O_7$
A
11
F
13
1
C
Jack
12
18
16
6
14
9
10
E
7
8
D
1
AlN
SiO_2
27R 21R 12H 15R
β'
XBL 873-1362

Figure 1

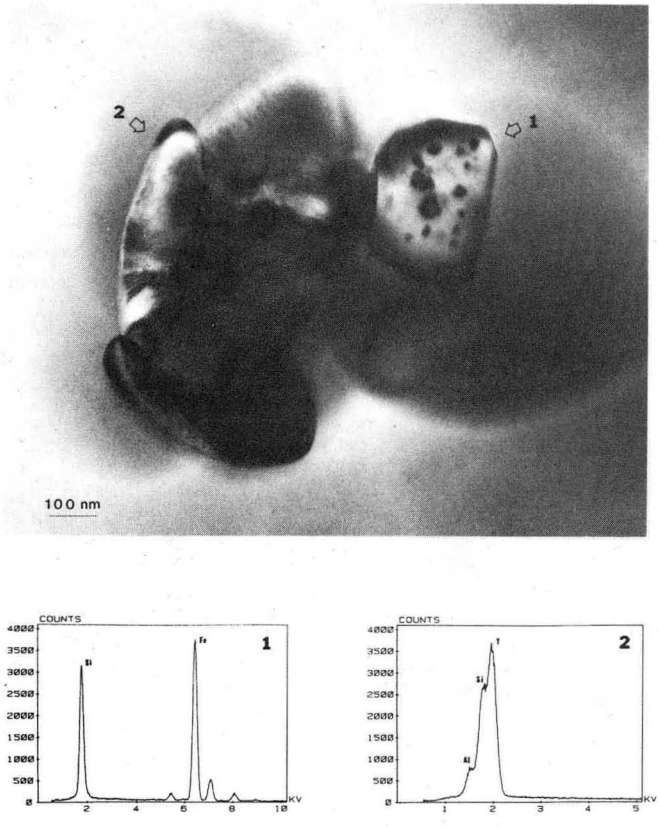

Figure 2

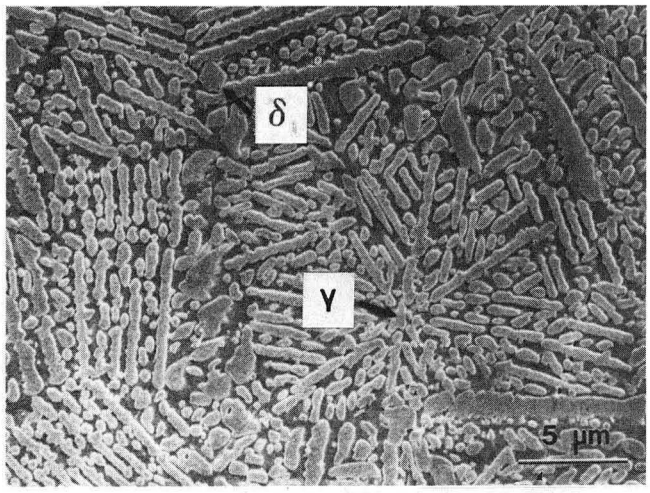

XBB 873-2527

Figure 3(A)

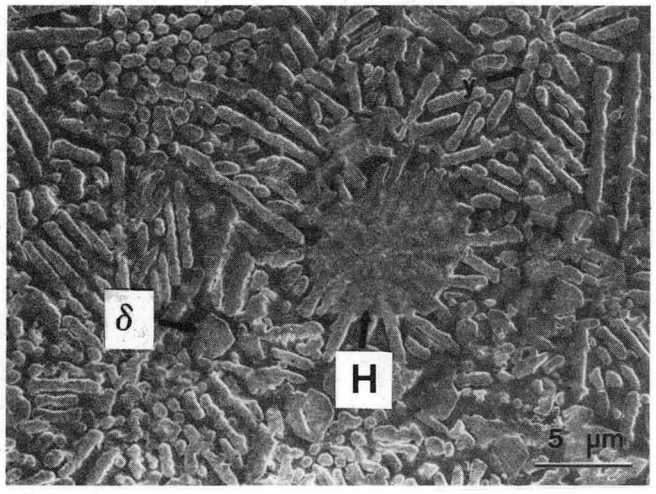

XBB 873-2528

Figure 3(B)

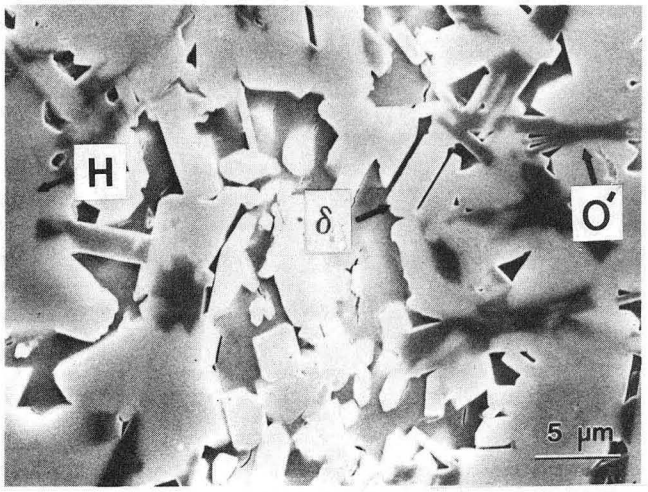

XBB 873-2529

Figure 3(C)

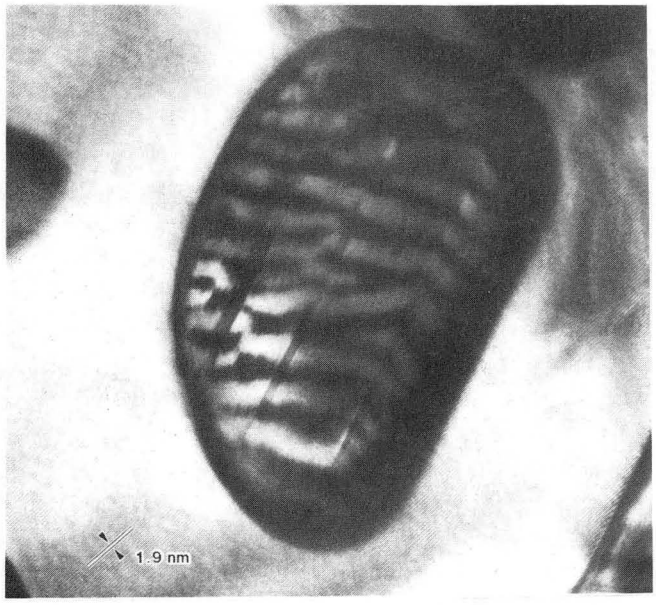

XBB 858-7009

Figure 4

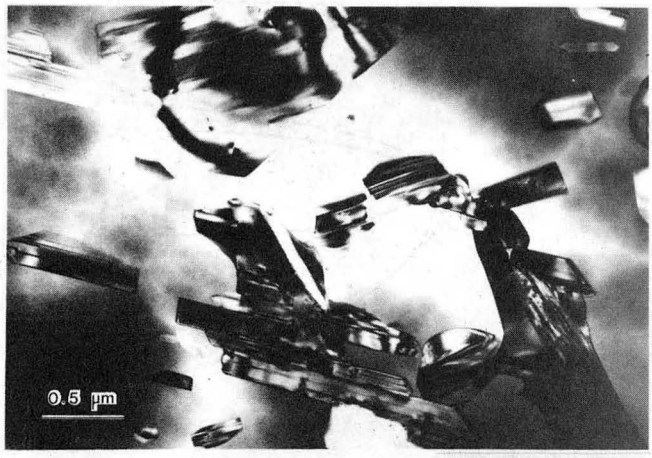

XBB 854-2596

Figure 5

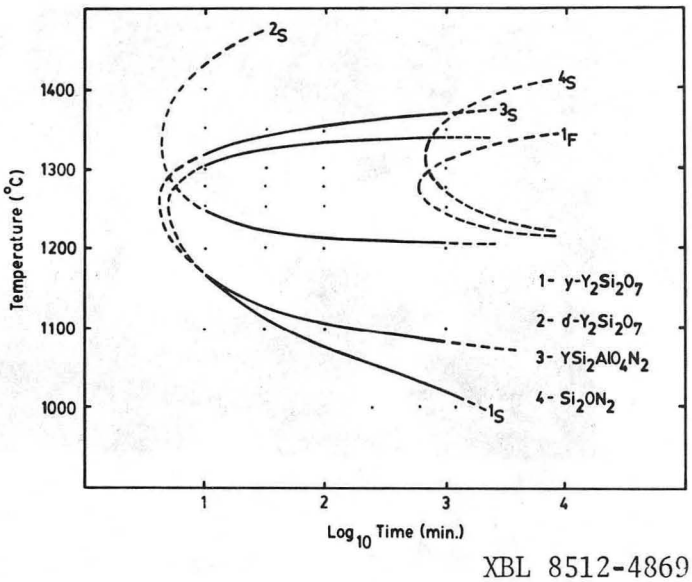

XBL 8512-4869

Figure 6

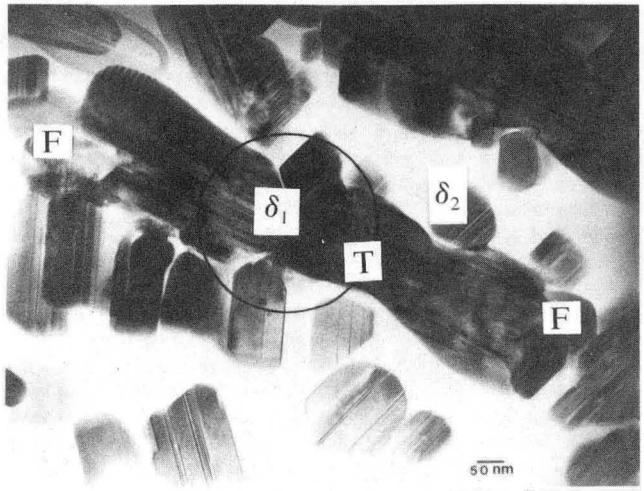

XBB 873-2530

Figure 7

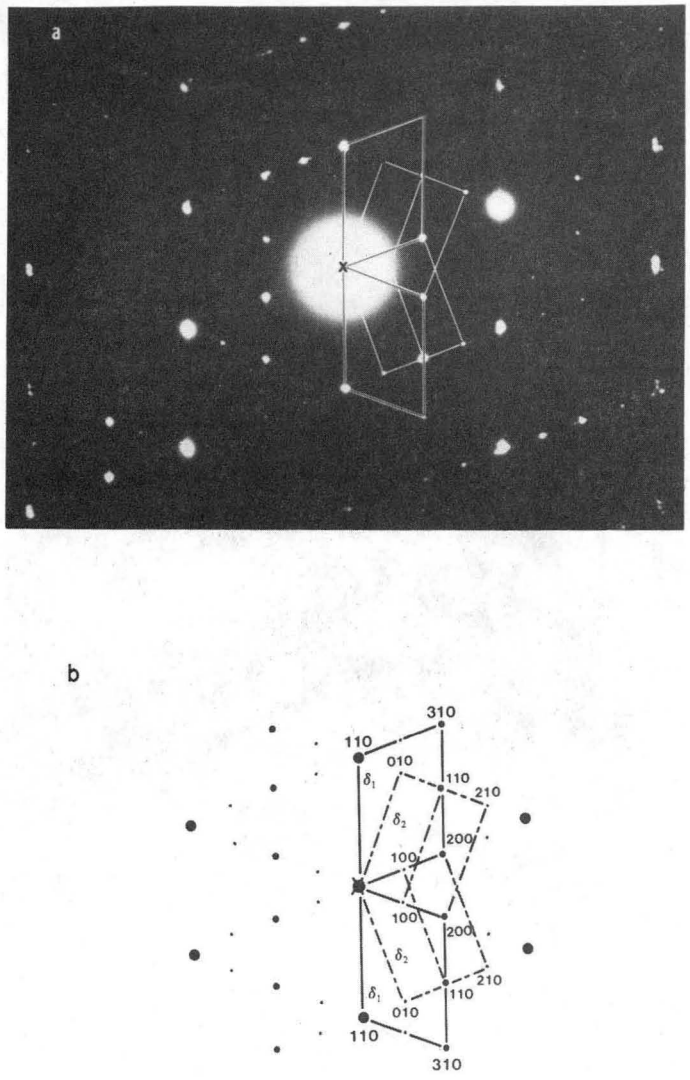

XBB 873-2531

Figure 8

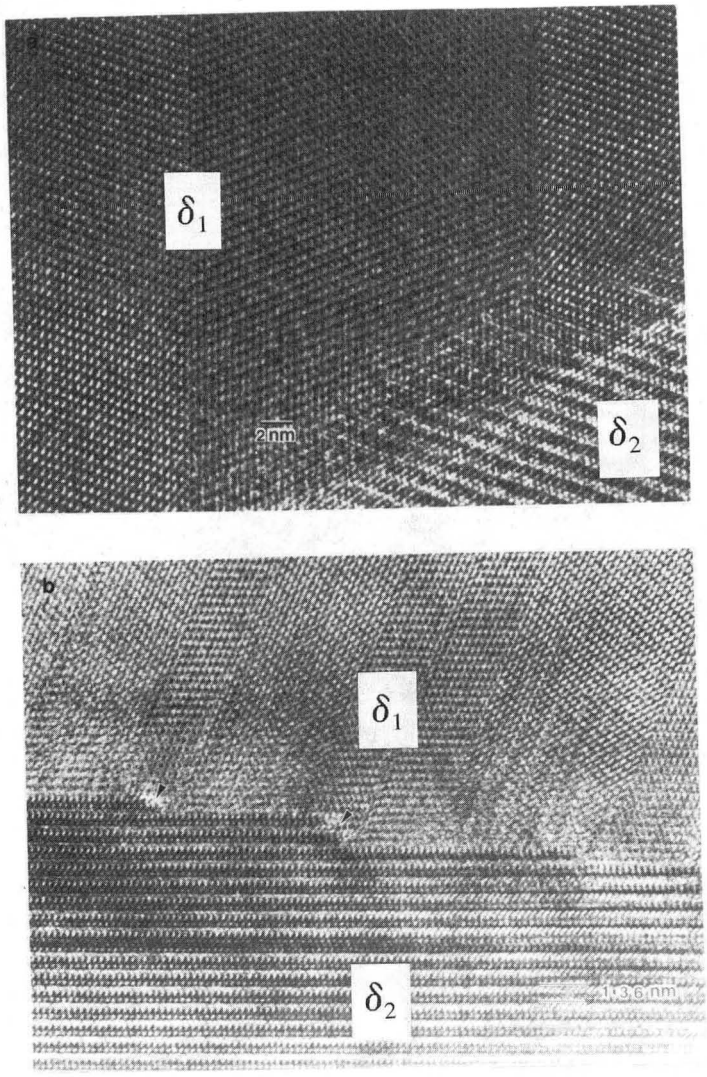

XBB 873-2532

Figure 9

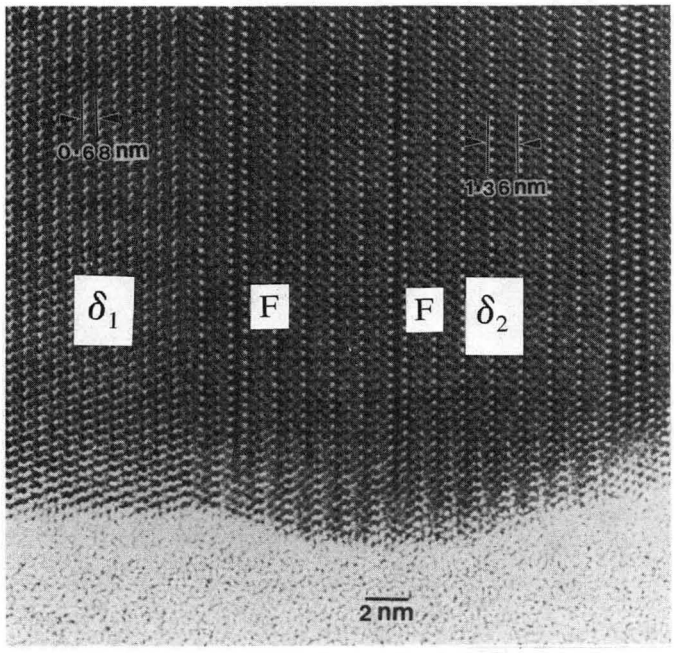

XBB 873-2533

Figure 10

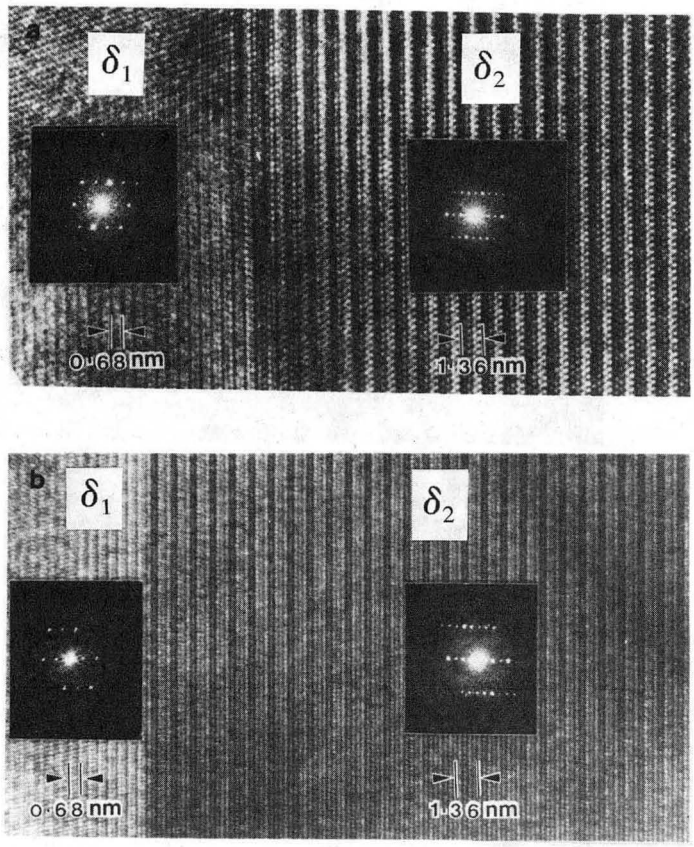

XBB 873-2534

Figure 11

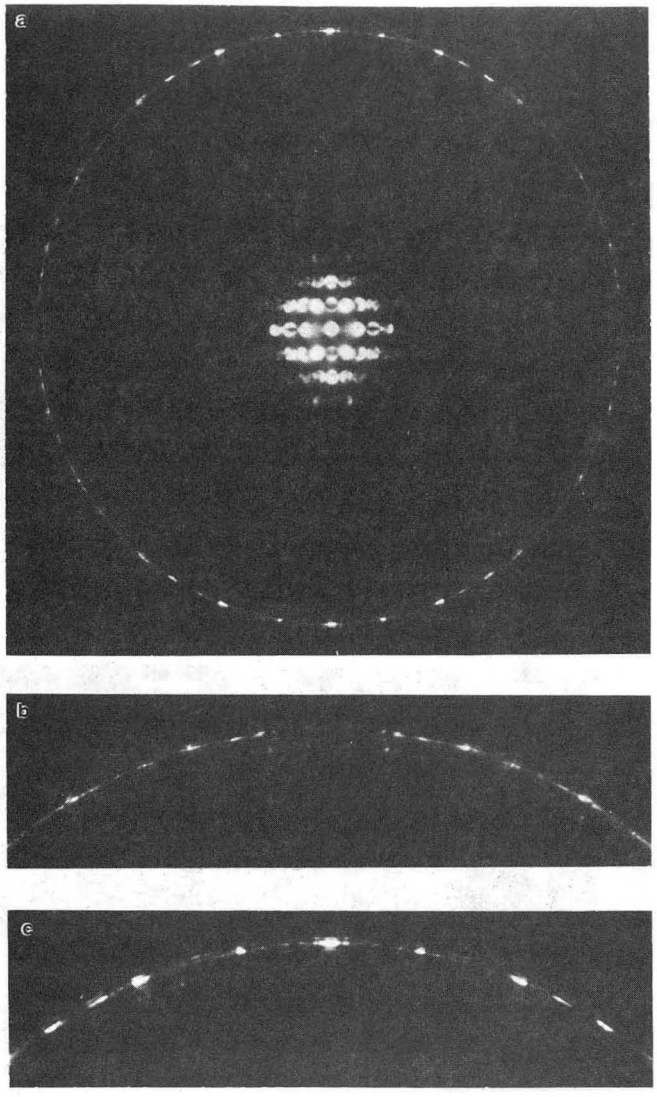

XBB 850-8445

Figure 12

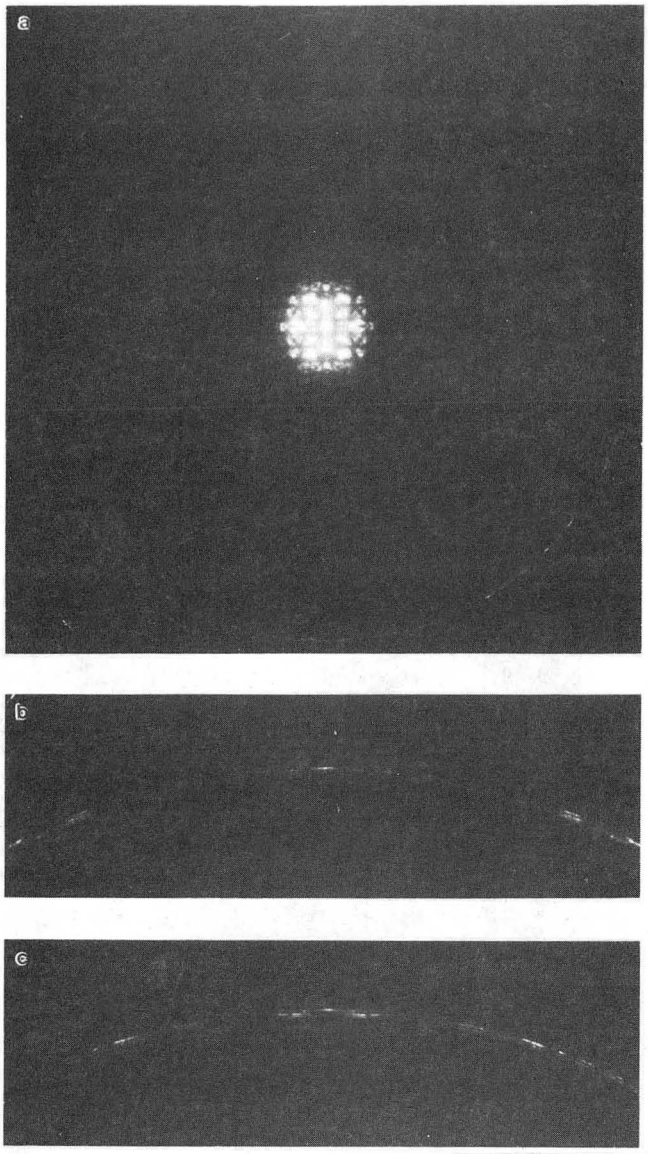

XBB 850-9326

Figure 13

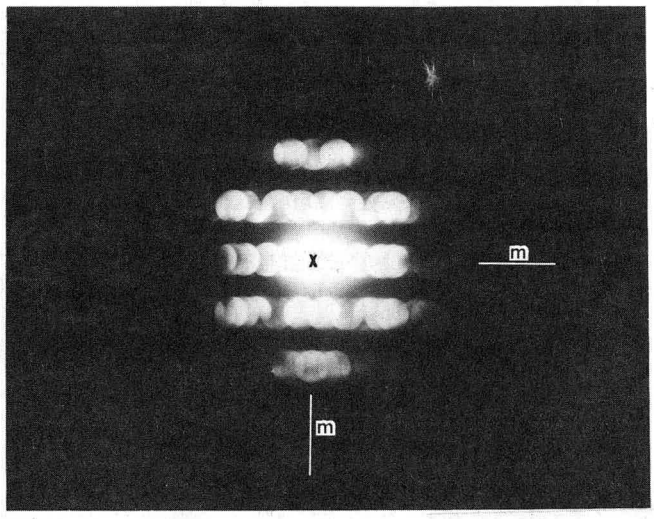

XBB 850-8035

Figure 14

This report was done with support from the Department of Energy. Any conclusions or opinions expressed in this report represent solely those of the author(s) and not necessarily those of The Regents of the University of California, the Lawrence Berkeley Laboratory or the Department of Energy.

Reference to a company or product name does not imply approval or recommendation of the product by the University of California or the U.S. Department of Energy to the exclusion of others that may be suitable.

LAWRENCE BERKELEY LABORATORY
TECHNICAL INFORMATION DEPARTMENT
UNIVERSITY OF CALIFORNIA
BERKELEY, CALIFORNIA 94720